Local-field-induced current noise in shape-limited self-doped polyaniline

Jiannan Bao, Yoichi Otsuka, Riko Etoh, Yuki Usami, Takuya Matsumoto

Department of Chemistry, Graduate School of Science, Osaka University, 560-0043 Toyonaka, Japan

E-mail: otsuka@chem.sci.osaka-u.ac.jp

E-mail: matsumoto-t@chem.sci.osaka-u.ac.jp

Abstract

Electronic noise generators are an essential component of molecular neuromorphic devices. To realize molecular noise generators with a high degree of freedom for design and integration into molecular devices, the utilization of the local electric field for the modulation of electrical conduction via a shape-limited conductive polymer is one promising strategy. Herein, a molecular noise generator composed of thin self-doped polyaniline (SPAN) lines is reported. SPAN lines fabricated via fountain pen lithography on SiO_2/Si substrates were found to generate current noise upon laser irradiation. This current noise exhibited white-noise-like power spectral density in the frequency range of 1–25 Hz and was independent of temperature. Multiple independent noise generation on the same substrate was also successfully demonstrated. The present results indicate that the noise generation mechanism involves the local modulation of hopping conduction via SPAN lines owing to the spatial proximity of the conduction path in the SPAN line to the surface photovoltage region of the SiO_2/Si interface. This on-site random noise generation in shape-limited conductive polymers is expected to be beneficial for the realization of molecular neuromorphic devices.

Introduction

We live in the presence of considerable noise originating not only from the outside world but also within our bodies. Noise is extensively utilized in natural stochastic systems, such as those for information processing in the human brain [1–4] and energy-efficient environmental signal detection by living creatures [5,6]. As the demand for greater computing capabilities continues to increase tremendously, neuromorphic devices based on neuron-inspired systems have been proposed [7,8].

One of the important phenomena for neuromorphic devices is stochastic resonance (SR), in which noise of an appropriate amplitude is added to a weak input signal to enhance the output response of nonlinear bistable or threshold systems [9]. Multiple-noise generators capable of producing different types of noise are also expected to be essential for the enhancement and conversion of weak signals [10]. SR is also widely applied in nonlinear sensing [11,12], and hence biomimetic devices utilizing SR are considered a promising pathway for linking complex biological information processing to next-generation non-von Neumann solutions [10,13].

Several groups demonstrated the SR by using molecular networks with the noise generated by an external function generator [14,15], but the use of typical box type function generators limits the integration of multiple noise generators on a chip. Other report

successfully realized generates electrical noise from the carbon-nanotube-based molecular devices [16], which is small enough for future integrationdevices. However, the noise is generated randomly with time and it is unable to control the on/off state of noise. In addition, the noise generation is a temperature sensitive process, thus the noise characteristics would be affected by unavoidable temperature change while operating [16-18].

For the development of molecular neuromorphic devices in which SR is highly utilized for information processing as in the human brain, three requirements for the fabrication of an appropriate molecular noise generator should be considered. First, multiple on-site independent noise generators should be realized using fabrication methods with a high degree of freedom for device design and integration. Second, the ON/Off state of the noise generation should be controlled and/or triggered according to the external conditions. Third, the noise generation should be independent of temperature to permit stable operation under various temperature conditions. To fulfill these requirements, we propose the strategy of utilizing shape-limited conductive polymers for on-site noise generation that can be controlled by local excitation. Because carrier transport in conductive polymers can be modulated by electric field, local current noise generation can be expected if the dimensions of the conduction path are narrow enough to permit modulation of the carrier conduction by a locally fluctuating electric field.

For the shape-limited conductive polymer, self-doped polyaniline (SPAN) is an attractive candidate. The hopping conduction between the localized metallic grains is affected by the gate voltage in the field-effect transistor structure [19]. Moreover, SPAN is soluble in a variety of solvents, permitting the fabrication of molecular patterns on a substrate via fountain pen lithography (FPL) [20–22]. In FPL, a solution containing the molecules is deposited onto the substrate using a position-controlled fine pipette. This technique permits both molecular patterning on the substrate and fabrication of molecular thin films at the nanoscale. The latter aspect is important because the conductive carriers in thin molecular patterns are expected to be strongly excited by the local electric field at the molecule/substrate interface owing to the limited volume of the conductive channel. Surface photovoltage is one promising phenomenon for generating a fluctuating local electric field. The irradiation of light onto an insulator/semiconductor interface results in the generation of electron-hole pairs and the diffusion of minority carriers toward the surface depletion regions. Consequently, the change of band-bending gives the fluctuated surface potential [23].

We herein report the fabrication and characterization of a molecular noise generator that relies on the sensitive response to a photoinduced local electric field at a SiO_2/Si interface. The ON/OFF control of noise generation in nanometer-thick line patterns of SPAN was realized by laser stimulation. The temperature-independent nature of this noise demonstrates the potential application of shape-limited SPAN lines to neuromorphic devices suitable for operation over a wide temperature range. Furthermore, the integration of multiple noise generators that work individually on-site was demonstrated. The results strongly suggest that the current noise generation technique is a local process that is suitable for next-generation neuromorphic computing devices.

Methods

Sample Preparation and Characterization

The SiO_2/Si substrates (boron-doped silicon wafers with a thickness of 525 ± 25 μm and a thermally grown 300 nm silicon dioxide layer, 0.1-100 Ω·cm, E&M) and quartz substrates (700 μm thickness, Daico) were processed by ultrasonic cleaning in acetone and UV/ozone treatment prior to use. Au/Cr electrodes (50 nm/10 nm thick, respectively) with a 30 μm gap size were fabricated via thermal evaporation onto the SiO_2/Si or quartz substrate. SPAN solution was prepared by mixing AquaPASS (SPAN) solution (Mitsubishi Rayon) with Milli-Q ultrapure water and methanol in a volume ratio of 1:4.5:4.5. Borosilicate nanopipettes

were fabricated using a thermal micropipette puller (PC-100, Narishige). The nanopipettes had an aperture size of approximately

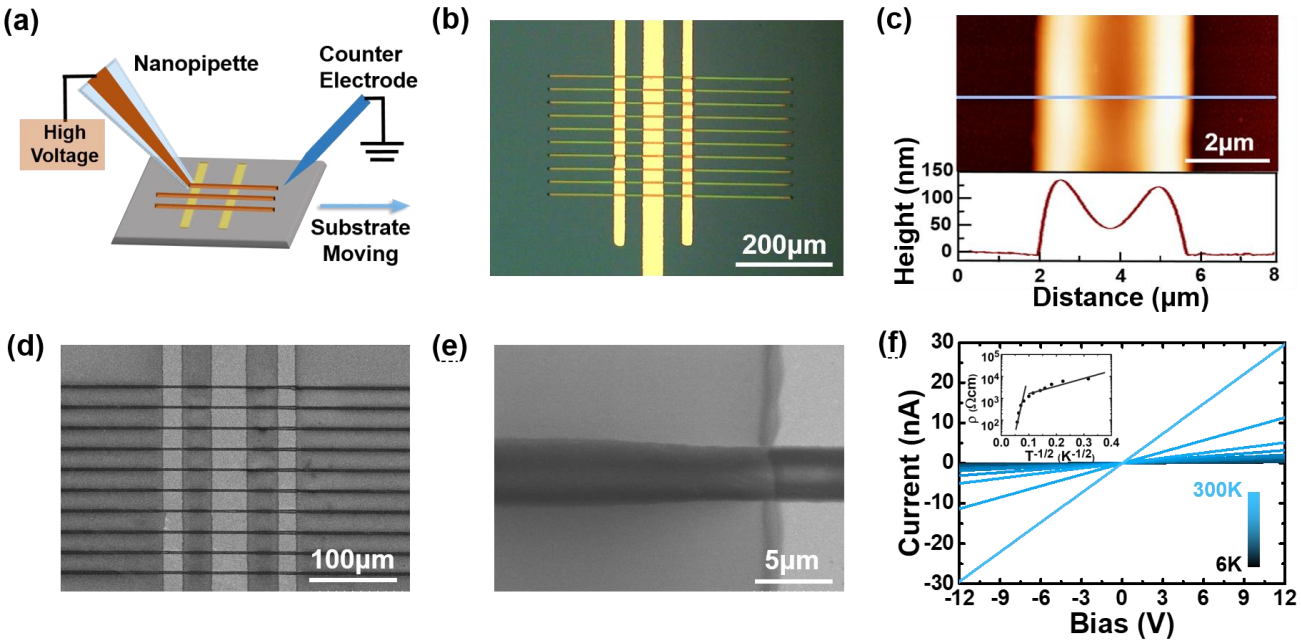

Figure 1. (a) Schematic illustration of the patterning of SPAN lines using a nanopipette. (b) SPAN line patterns observed by optical microscopy. (c) AFM image of a single SPAN line and a representative cross-sectional profile. (d) SEM image of SPAN line patterns, 300x magnification. (e) SEM image of a single line pattern, 6000x magnification. (f) Representative *I*–*V* characteristics of SPAN lines on a SiO_2/Si substrate in the temperature range of 6–300 K under a pressure of 10^{-4} Pa. The inset displays a semi-logarithmic plot of the resistivity ρ versus $T^{-1/2}$, where the solid lines indicate the fitting results for the high-temperature region (200–300 K) and low-temperature region (10–50 K) obtained using equation (1).

500 nm, as confirmed by SEM (SU-6600, Hitachi) using an acceleration voltage of 5 kV. The surface of each nanopipette was coated with gold by ion sputtering (JFC-1500, JEOL) to prevent local charging. The bias voltage applied to the SPAN solution in the nanopipette was 300 V relative to the grounded counter electrode to realize stable and continuous deposition of the solution onto the substrate. This procedure is important because the charged SPAN solution was dispensed from the nanopipette aperture owing to the electrostatic force. The scanning speed was 50 μm/s. The images of line patterns were taken by optical microscope (BX51M, Olympus) and SEM (SU-6600, Hitachi) using an acceleration voltage of 3 kV. The height of the SPAN lines was measured using tapping-mode AFM (JSPM-4200, JEOL) with a silicon cantilever probe (NCH, Nanoworld, resonance frequency: 330 kHz).

Electrical Measurement and Data Analysis

The electrical current was characterized using a source meter (2636B, Keithley) equipped with a high-vacuum prober (ST-500, Janis) over a temperature range of 6–300 K under a pressure of 10^{-4} Pa. The time interval during the *I*–*t* measurements was 20 ms (37 ms for the two-device measurement). The high and low ranges of the current were set to 10^{-7} and 10^{-14} A, respectively (for the measurement of the bare substrate, auto ranging was used), and the number of power line cycles was set to 1. Laser irradiation was performed using a 532 nm continuous-wave laser diode (Stradus 532, Vortran) operating at a fixed laser power of 5 mW in the modulation mode. An optical fiber was used to guide the laser light into the high-vacuum prober, and the size of the illuminated area was 1 cm^2. The on/off states of the laser

and the data acquisition system (NI 6341, National Instruments) were controlled using a custom-built LabVIEW program. The *I*–*t* data were analyzed using Fourier transformation (Origin 9.1) to obtain the PSDs. To avoid the influence of transient current, the *I*–*t* data 10 s after switching the laser were used in the PSD analysis.

Results and discussion

Surface structure and I–V characteristics of SPAN lines

Figure 1(a) presents a schematic overview of the device fabrication procedure. SPAN lines were fabricated using a nanopipette and custom-built FPL apparatus. The apex of a nanopipette filled with SPAN solution was contacted to the SiO_2/Si substrate and moved over gold electrodes situated at an interelectrode distance of 30 μm. A bias voltage was applied between the SPAN solution and counter electrode to induce continuous deposition of the solution. In a typical device, 10 SPAN lines were patterned over the electrodes.

The SPAN lines were examined using optical microscopy and atomic force microscopy (AFM). Lines with a length of 500 μm, a nominal width of 4 μm were fabricated between the electrodes (figure 1(b)). The average height of each line was approximately 100 nm (figure 1(c)). The double peaks in the cross-sectional profile were ascribed to the coffee-ring effect and were also observed by optical microscopy (figure S1). Figure 1(d) and 1(e) show the general and detailed view of SPAN lines characterized by SEM. The line width on Au electrode and SiO_2/Si surface was slightly different with a nominal difference less than 1 μm, which would be due to the changes of mechanical contact between a glass capillary and a substrate or an electrode due to their height difference (Au electrode was 50 nm higher than the substrate). The meniscus shape of SPAN solution between a probe and a surface would be changed when the angle of probe apex was changed. The other possibility is the wettability of SPAN solution on a surface. Figure 1(f) presents the current–voltage (*I*–*V*) characteristics and temperature dependence of the resistivity (ρ) of the SPAN lines. The linear *I*–*V* characteristics in the temperature range of 6–300 K are typical of high-concentration SPAN films [24]. In general, the conduction mechanism in polyaniline can be described by Mott's variable-range hopping model. The temperature dependence of ρ and the activation energy (E_a) can be expressed by equations 1 and 2, respectively [24–27]:

$$\rho = \rho_0 \exp\left((T_0 / T)^{1/2}\right) \tag{1}$$

$$E_a = \frac{1}{2} k_B T_0^{1/2} T^{1/2} \tag{2}$$

where ρ_0, T_0, and k_B are the high-temperature limit of resistivity, Mott's characteristic temperature, and theBoltzmann constant, respectively. The solid lines in the plot shown in the inset of figure 1(d) are the fitting results for the high-temperature region (200–300 K) and low-temperature region (6–50 K) obtained using Equation 1. The values of T_0 and E_a were 1.8×10^4 K and 100 meV for the high-temperature region and 45 K and 0.7 meV for the low-temperature region, respectively. These values are similar to previous results reported for polyaniline [24, 27–29]. The two different values of E_a indicate the presence of the metallic grains and disordered regions inside the shape-limited SPAN lines. In the metallic grains, the SPAN molecules are ordered to form the free carriers,

whereas the disordered regions act as insulating layers between the metallic grains, resulting in the occurrence of hopping conduction

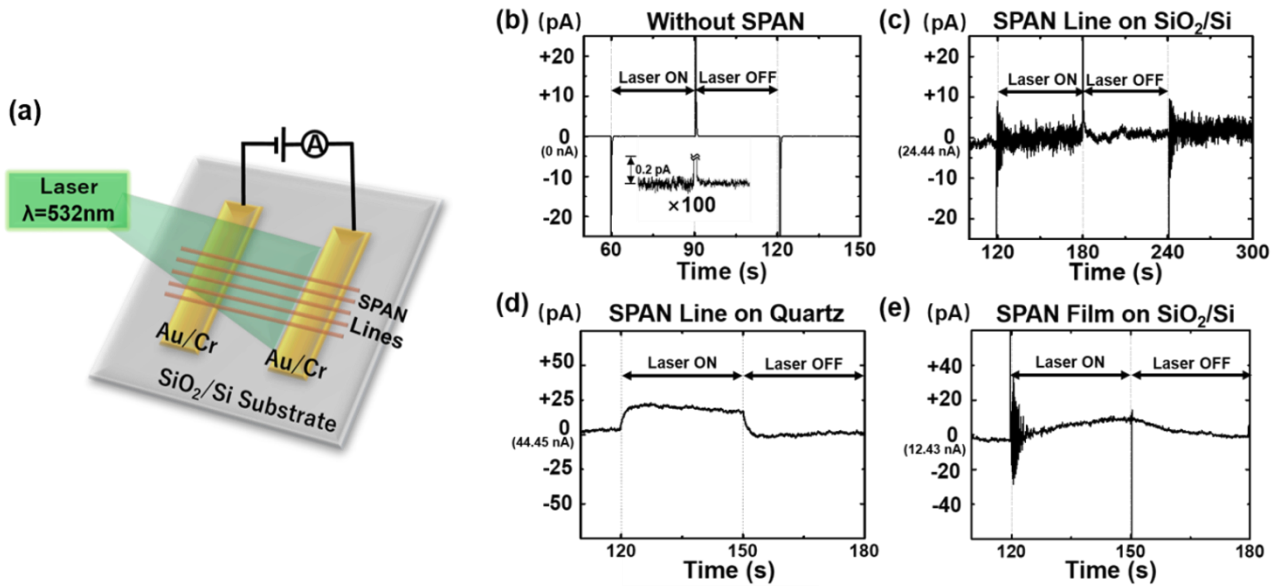

Figure 2. (a) Schematic illustration of the electrical measurement of current noise under laser irradiation. (b) Representative *I*–*t* plot of the substrate prior to the patterning of SPAN lines. The interval of laser irradiation was 30 s. The inset shows an enlarged view with the *y* axis magnified by a factor of 100. (c) Representative *I*–*t* plot of a SPAN line on a SiO_2/Si substrate. The interval of laser irradiation was 60 s. (d) Representative *I*–*t* plot of a SPAN line on a quartz substrate. (e) Representative *I*–*t* plot of a drop-cast SPAN film on a SiO_2/Si substrate. In (b)–(e), the electrical current was measured under a bias voltage of 1 V, a pressure of 10^{-4} Pa and a temperature of 300 K.

between the metallic grains.

The presence of the metallic grains in the shape-limited SPAN lines is essential for the on-site current noise because the electric potential of each metallic grain in a SPAN line can be modulated efficiently by a local electric field. A comparison of the current noise generation between the SPAN lines and a SPAN film will be presented.

Current noise generation with laser irradiation

Figure 2(a) shows a schematic illustration of the current noise measurement. The electrical current was measured in the presence and absence of laser irradiation. All measurements were performed under vacuum conditions. A current–time (*I*–*t*) plot of the bare electrodes on a substrate prior to the patterning of the SPAN lines is presented in figure 2(b), in which a current fluctuation of 0.1 pA was measured during laser irradiation. The low current noise measured for the bare Au electrodes on the SiO_2/Si substrate (figure 2(b)) can be considered as local charge accumulation due to the surface photovoltage.

Following this measurement, SPAN lines were patterned between the same electrodes and the electrical current was measured. The *I*–*t* plot of the SPAN lines at a bias voltage of 1 V revealed a detectable current noise upon laser irradiation. As shown in figure 2(c), the photoinduced transient current was measured in the first 5 s after laser irradiation, whereas in the subsequent period the current noise exhibited a relatively stable amplitude. The latter period of stable current noise was analyzed in this study because it was reproducible. The current noise amplitude was considerably larger than that of the bare Au electrodes. This current noise generation was observed in 79 out of 192 devices, with variable noise amplitude from sample to sample. These results suggest that the current noise originated from the SiO_2/Si interface and was enhanced by the SPAN molecules.

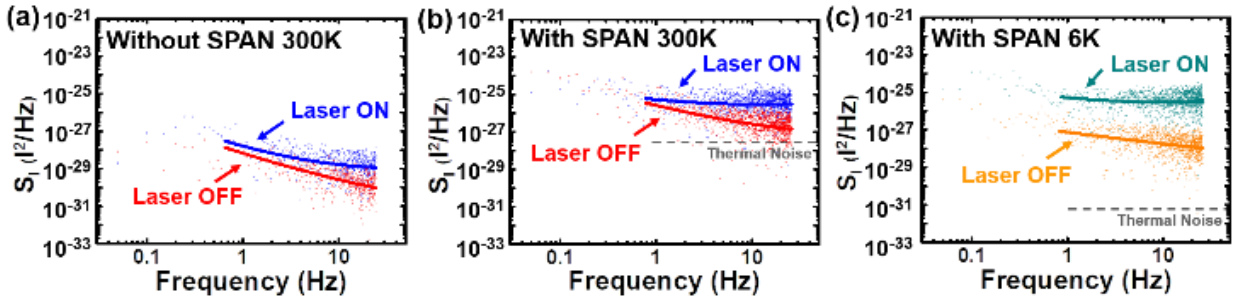

Figure 3. PSDs of the current noise (a) without and (b) with SPAN lines, which were obtained from the *I*–*t* plots shown in Figures 2(b) and (c), respectively. (c) PSD of the current noise with SPAN lines. The *I*–*t* plot was measured at 6 K with a bias voltage of 1 V, a laser pulse of 60 s and a pressure of 10^{-4} Pa. In each plot, the solid lines indicate the fitting results in the frequency range of 1–25 Hz and the dashed gray lines indicate the corresponding thermal noise level. The thermal noise levels at 300 and 6 K were estimated to be 4×10^{-28} and 4×10^{-32} A^2/Hz, respectively, using Equation (3).

To evaluate the influence of the substrate, the *I*–*V* and *I*–*t* characteristics were also measured for SPAN lines on quartz substrates. Among 204 samples, we did not detect current noise in either the presence or absence of laser irradiation (figure 2(d)), which indicates that the current noise generation originated from the intrinsic properties of the SiO_2/Si substrate. To evaluate the importance of line patterning, the *I*–*t* characteristics of drop-cast SPAN films on SiO_2/Si substrates were also measured. Among 32 devices, no device exhibited stable current noise (figure 2(e)). This result demonstrates that a constrained sample thickness and area on the SiO_2/Si substrate were crucial for current noise generation. The results shown in figures 2(d) and (e) also show the improbability of current noise generation at the electrode/substrate interface or contact noise from the SPAN/electrode interfaces, the photo-excited carriers of SPAN and the surface plasmon effect of gold electrode because no significant differences were detected from these samples in the presence and absence of laser irradiation. We also tested a broken sample in which the SiO_2 layer was damaged to confirm that the noise generation was not attributable to leakage current through the Si substrate (figure S2). These results confirmed that the essential requirements for the current noise generation were exposure to laser irradiation and the shape-limited SPAN lines on a SiO_2/Si interface.

To examine the characteristics of the noise, the power spectral density (PSD) was compared for samples without SPAN (SiO_2/Si substrate with Au/Cr electrodes) and with SPAN lines. As shown in figure 3(a), the PSD of the bare SiO_2/Si substrate exhibited 1/*f* characteristics in the absence of laser irradiation. In the presence of laser irradiation, the PSD increased with respect to 1/*f* in the

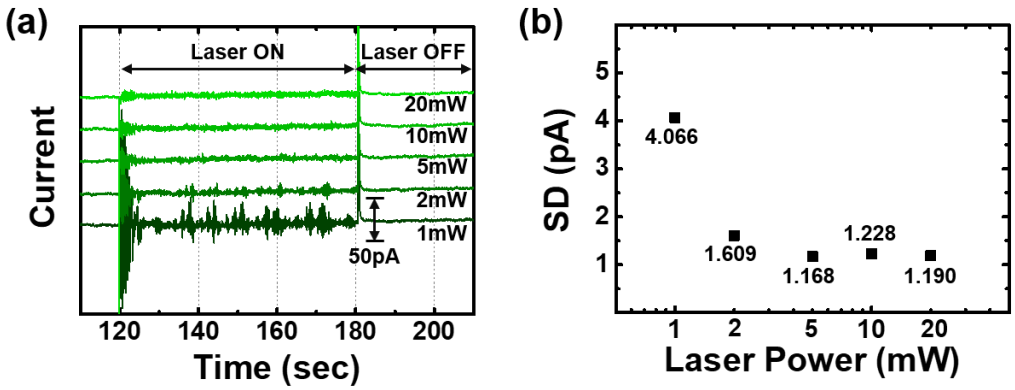

Figure 4. (a) *I*-*t* plots of the current noise with different laser power. The *I*–*t* plot was measured at room temperature with a bias voltage of 1 V, a laser pulse of 60 s and a pressure of 10^{-4} Pa. (b) Standard deviation of current noise with different laser power.

high-frequency region. Following the deposition of the SPAN lines on the same substrate, the noise amplitude in the absence of laser irradiation was significantly greater than that observed for the bare substrate (figure 3(b)). This was ascribed to the current dependence of 1/*f* noise. The PSD of 1/*f* noise ($S_I(1/f)$) is typically proportional to I^x in ohmic systems, where *I* and *x* are the current and a variable parameter, respectively [30,31]. The 1/*f* noise was slightly curved in the higher-frequency region, which was attributed to thermal noise. The thermal noise level (S_I) was estimated to be 4×10^{-28} A^2/Hz (dotted line in Figure 3(b)) using Equation 3:

$$S_I = 4k_B T/R \tag{3}$$

where k_B, *T*, and *R* are the Boltzmann constant, temperature, and sample resistance, respectively. Upon laser irradiation, a white-noise-like PSD was observed in the frequency range of 1–25 Hz, which indicates that the shape-limited SPAN lines played a significant role as the current noise generator upon laser irradiation.

To further investigate the properties of the current noise with the SPAN lines, the temperature dependence was examined. figure 3(b) and figure 3(c) present the PSDs of the SPAN lines at 300 and 6 K, respectively. In the absence of laser irradiation, the noise exhibited a 1/*f* shape at both temperatures, with a positive shift at 300 K owing to the greater conductivity of SPAN lines at higher temperatures and the current dependence of 1/*f* noise. In contrast, in the presence of laser irradiation, white-noise-like PSDs were observed with negligible temperature dependence in the range of 6–300 K. More intuitively, plots of the current noise during the *I*–*t* measurements are shown directly in Figure S3. The average noise amplitude remained almost constant irrespective of temperature, although the current varied by two orders of magnitude from 6 to 300 K. These results indicate that the nominal current was thermally sensitive owing to the occurrence of hopping conduction, whereas the current noise generation was independent of the thermal process.

The *I*–*t* characteristics of the SPAN lines were also examined under various laser powers (figure 4(a)). Under a weak laser power (1 mW), a wider range of current noise fluctuation was observed. As the laser power was increased, the signal amplitude of the current noise became more uniform. The standard deviation of current noise in *I*-*t* data was calculated to show the range of fluctuation more intuitively. As depicted in figure 4 (b), the larger standard deviation of 1 mW and 2 mW *I*-*t* data indicated the fluctuation range was wider at lower laser power. At 5 mW, 10 mW and 20 mw, standard deviation data shown no obvious difference, whereas the minor drift might be due to the change in nominal current level. These results can be explained by the degree of band bending at the SiO_2/Si interface. The variation of the current noise over time indicates that the band bending was far from saturation and that an inhomogeneous local electric field was formed under weak laser irradiation. Upon increasing the laser power, the band bending became saturated to form a flat band [32], resulting in stable current noise with negligible spikes in the *I*–*t* plots.

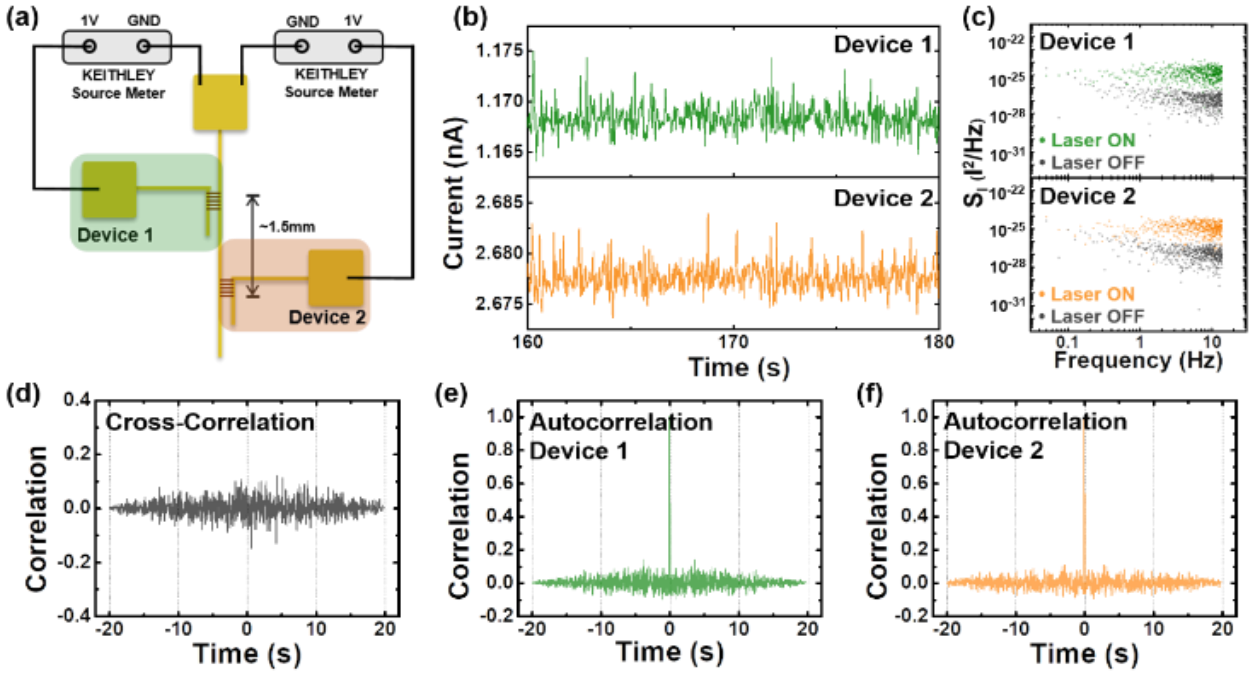

Figure 5. (a) Schematic illustration of the simultaneous *I*–*t* measurement of two isolated devices on the same substrate. (b) Comparison of the *I*–*t* characteristics of the two devices under laser irradiation with a bias voltage of 1 V and a sampling interval of 37 ms. (c) Comparison of the PSDs of the current noise generated in the two devices. (d) Cross-correlation of the *I*–*t* data for the two devices. (e), (f) Autocorrelation of the *I*–*t* data for each device. The electrical current was measured under a bias voltage of 1 V, a pressure of 10^{-4} Pa and a temperature of 300 K.

The influence of the electric field on the electrical current in the SPAN line was also evaluated by controlling the gate voltage. The current flow in the SPAN molecules was sensitive to changes in the gate voltage but remained stable at a constant gate voltage, which suggests that the variation of the local electric field due to the fluctuating surface photovoltage at the SiO_2/Si interface was able to affect the carrier transport in the SPAN line (figure S4).

Demonstration of on-site current noise generation

To further examine the on-site current noise generation, the *I*–*t* characteristics of two devices on the same substrate were measured simultaneously. Synchronization of the current noise from the two devices would indicate that the noise generation originated from a general mechanism such as fluctuation of the laser power, whereas a lack of synchronization would suggest a local mechanism of noise generation. The level of synchronization was demonstrated by cross-correlation and autocorrelation function, which is commonly used to evaluate the relationship between multiple and/or time series signals [33, 34]. As depicted in figure 5(a), the two samples were fabricated on the same SiO_2/Si substrate and their current noise was measured simultaneously using two source measure units. The distance between two devices was approximately 1.5 mm. figure 5(b) and figure 5(c) show the *I*–*t* characteristics and corresponding PSDs of the two devices. The PSDs of the two devices exhibited similar behavior in the frequency range of 0.1–10 Hz. The correlation coefficient of the *I*–*t* characteristics was calculated to be 0.094, and the cross-correlation of the current noise from the two devices throughout the entire time range was less than 0.1 (figure 5(d)). This lack of correlation demonstrates that the current noise from the two devices was independent. These distinctive time-resolved noise properties of two devices on the same substrate indicate that the current noise was not attributable to a general effect such as fluctuation of the laser power but rather local modulation of the electronic states

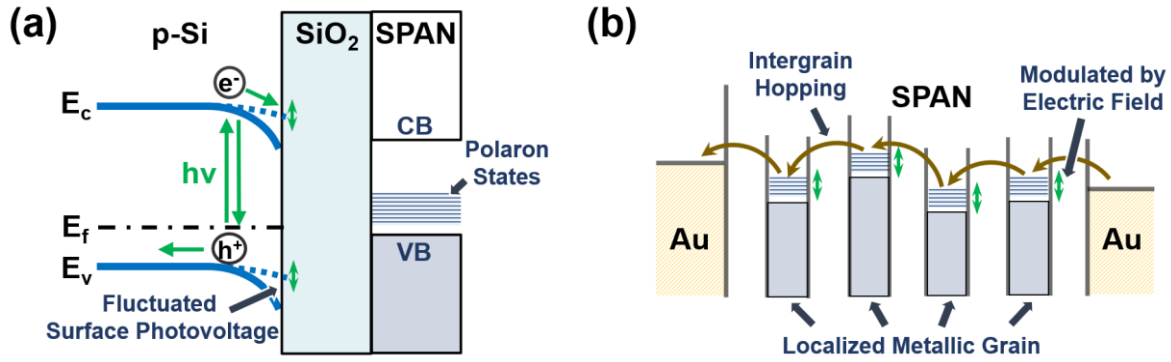

Figure 6. (a) Schematic illustration of the electric field generated by the fluctuation of the surface photovoltage at the SiO_2/Si interface. Green arrows indicate carrier separation/accumulation upon laser irradiation and blue double-headed arrows indicate the fluctuating surface photovoltage generated by carrier separation at the SiO_2/Si interface. The metallic grains, which are formed inside SPAN, is modulated by the adjacent electric field due to the surface photovoltage. (b) Schematic illustration of

The autocorrelation data of the two devices (figure 5(e) and figure 5(f)) also revealed little correlation, indicating that the current noise generation was a short-term nonperiodic phenomenon, although the relaxation time could not be determined under these conditions owing to the sampling interval of 37 ms. Therefore, our results demonstrate that the current noise was generated locally and independently in the SPAN lines.

Proposed model of current noise generation

Regarding the mechanism of noise generation, a brief summary of all experimental results is necessary. By the comparison between different device configurations (figure 2), essential conditions for the noise generation phenomena were confirmed, which are optical stimulation, shape-limited SPAN molecules and SiO_2/Si interface. Put it in another way, the current noise is generated from the interplay between photoexcited carriers in SiO_2/Si and the electrical conduction in SPAN lines.

The temperature dependence measurements clarified that the current level is thermally sensitive while the current noise property is thermally insensitive (figure 3). The dominant conductive mechanism in SPAN lines is confirmed as hopping conduction via metallic grains, which is a thermally sensitive process.

The laser power dependence measurements indicated a transition from the metastable current noise with larger amplitude to the stable current noise with smaller amplitude with increasing the laser power (figure 4). This result also supports the effect of surface photovoltage onto the current noise. As the amount of photogenerated charge carriers at the SiO_2/Si interface are limited by the recombination rate [35], saturated electrical potential is generated at high light intensities. Under the saturated condition, the current noise amplitude would be suppressed because of a little fluctuation in surface potential.

At last, properties of two devices located at a same substrate under identical laser irradiation confirmed that the current noises are independent from each other, thus indicated a local effect is involved in the noise generation mechanism and excluded the possibility of laser power fluctuation.

Based on the above experimental results, we propose the model of current noise generation. figure 6(a) presents a schematic illustration of the local electric field formed by the surface photovoltage at the SiO_2/Si interface. The excited carriers formed upon laser irradiation result in non-equilibrium carrier separation and accumulation, and the varying carrier motion affords a noisy surface photovoltage that generates a fluctuating local electric field at the SiO_2/Si interface. The use of 5mW laser power in figure 3 and figure 5 was sufficient to saturate the band bending of p-Si at the SiO_2/Si interface.

With respect to the current noise generation in a SPAN line, the hopping conduction via the metallic grains in the SPAN line undergoes modulation due to the fluctuating local electric field at the SiO_2/Si interface, as shown in figure 6(b). In other words, the minute fluctuation of surface photovoltage is sensed by the metallic grains of SPAN lines, and the electrical current is modulated. The current level is determined by the variable range hopping conduction, thus it is temperature dependent. On the other hand, the current noise amplitude is temperature independent because of the saturated surface photovoltage at the SiO_2/Si interface. The hopping probability P in the Mott's variable-range hopping model has the form:

$$P \sim \exp[-\frac{2R}{a} - \frac{\Delta E}{k_B T}] \quad (4)$$

where R is hopping distance, a is the localization length, k_B is the Boltzmann constant and ΔE is the activation energy. [36] In the present study, the hopping probability P would be changed by the modulation of average activation energy barrier by surface photovoltage and the current noise is generated. The other parameters such as R and a can be treated as constant under each temperature condition (figure 3).

Confinement of the width and thickness of the SPAN line is important because of the limited area of surface photovoltage. As the diffusion length of the minority carriers in SiO_2/Si substrates is considered to be approximately several hundreds of micrometers [37], the area of the fluctuating electric field should exceed the width of the SPAN lines (3–6 μm). When a fluctuating electric field is generated in the vicinity of the SPAN lines, modulation of the electric potential should occur efficiently. In contrast, during the measurements of the SPAN film, the electrical conduction was averaged and hence little current noise was detected (figure 2(e)). These experimental results would support the proposed model in which the modulation of electric field is generated locally by surface photovoltage. The PSD spectrum from 1 Hz to 25 Hz would be reasonable because a surface photovoltage can respond up to the order of hundreds Hz considering the resistivity of substrate [38].

The inhomogeneity of surface photovoltage on Si wafer has been characterized by mapping minority carrier distribution length [39]. The time-resolved Kelvin probe force microscopy can be used to acquire the time-resolved information of surface potential and carrier lifetime [40, 41]. Although the time-resolved imaging in an order of picoseconds is not achieved to measure the dynamic change of excited carriers, these techniques can be applied visualize the spatial resolution of dynamic change due to local carriers inside conductive polymers [41].

As shown in figure 5, we observed the independet on-site generation of current noise in SPAN lines separted by a distance of 1.5 mm. On the basis of the diffusion length, the distribution area of the fluctuating electric field can be considered as several hundreds of micrometers. Therefore, it is expected that the spacing between each SPAN line could be further reduced to permit the integration of multiple noise generators on a single chip.

Conclusions

In conclusion, we have demonstrated the on-site generation of current noise using nanometer-thick SPAN lines deposited on a SiO_2/Si substrate. The noise generation is considered to originate from modulation of the hopping conduction through the shape-limited SPAN with a fluctuating local electric field due to the surface photovoltage at the SiO_2/Si interface. It should be emphasized that the patterning of conductive polymers using FPL is a promising technique for creating shape-limited molecular devices in which the interaction between the molecular electronic state and the surrounding electric field is effectively exploited. Compared with existing material-based noise generators, the on/off state controllable and temperature insensitive feature are realized for the first

time, as far as we know. Such on-site independent noise generation demonstrated here represents a potential route for the realization of artificial noise-stimulated microelectronic systems inspired by living creatures.

References

[1] M. S. Samoilov, G. Price, and A. P. Arkin, 2006, *Sci. STKE*., re17.

[2] T. Mori and S. Kai, 2002, *Phys. Rev. Lett.*, **88**, 218101.

[3] I. Hidaka, D. Nozaki, and Y. Yamamoto, 2000, *Phys. Rev. Lett.*, **85**, 3740-3743.

[4] T. Aihara, K. Kitajo, D. Nozaki, and Y. Yamamoto, 2010, *Chem. Phys.*, **375**, 616-624.

[5] J. Douglass, L. Wilkens, E. Pantazelou and F. Moss, 1993, *Nature*, **365**, 337–340.

[6] D. F. Russell, L. A. Wilkens and F. Moss, 1999, *Nature*, **402**, 291–294.

[7] D. Hassabis, D. Kumaran, C. Summerfield, M. Botvinick, 2017, *Neuron*, **95**, 245-258

[8] S. K. Esser, P. A. Merolla, J. V Arthur, A. S. Cassidy, R. Appuswamy, A. Andreopoulos, D. J. Berg, J. L. Mckinstry, T. Melano, D. R. Barch, C. Nolfo, P. Datta, A. Amir, B. Taba, M. D. Flickner, D. S. Modha, 2016, *PNAS*, **113**, 11441-11446.

[9] R. Benzi, A. Sutera, A. Vulpiani, 1981, *J. Phys. A: Math. Gen.*, **14**, L453-L457.

[10] J. J. Collins, C. C. Chow, and T. T. Imhoff, *Nature*, **1995**, 376, 236-238.

[11] F. Moss, L. M. Ward, W. G. Sannita, 2004, *Clinical Neurophysiology*, **115**, 267-281

[12] P. Jung and P. Hanggi, 1991, *Phys. Rev. A*, **44**, 8032-8042

[13] Y. Burgt, A. Melianas, S. T. Keene, G. Malliaras, 2018, *Nat. Electron.*, **1**, 386-397.

[14] Y. Hirano, Y. Segawa, T. Kawai, and T. Matsumoto, 2013, *J. Phys. Chem. C*, **117,** 140-145.

[15] Y. Hirano, Y. Segawa, T. Kuroda-Sowa, T. Kawai, and T. Matsumoto, 2014, *Appl. Phys. Lett.*, **104**, 233104.

[16] H. Fujii, A. Setiadi, Y. Kuwahara, and M. Akai-Kasaya, 2017, *Appl. Phys. Lett.*, **111**, 133501.

[17] H. Tanaka, M. Akai-Kasaya, A. Termehyousefi, L. Hong, L. Fu, H. Tamukoh, D. Tanaka, T. Asai, and T. Ogawa, 2018, *Nat. Commun.*, **9**, 1-7.

[18] A. Setiadi, H. Fujii, S. Kasai, K.I. Yamashita, T. Ogawa, T. Ikuta, Y. Kanai, K. Matsumoto, Y. Kuwahara, and M. Akai-Kasaya, 2017, *Nanoscale*, **9**, 10674-10683.

[19] C. Kuo, S. Chen, G. Hwang, H. Kuo, 1998, *Synth. Met.*, **93**, 155-160

[20] T. Yeshua, S. Weinberger, H. Taha, A. Lewis, M. Layani, C. Lehmann, S. Reich, C. Sukenik, and S. Kokotov, 2014, *Microsc. Anal.*, **28**, 11-15.

[21] T. Yeshua, M. Layani, R. Dekhter, U. Huebner, S. Magdassi, A, Lewis, 2018, *Small*, **14**, 1702324

[22] A. Lewis, Y. Kheifetz, E. Shambrodt, A. Radko, E. Khatchatryan, and C. Sukenik, 1999, *Appl. Phys. Lett.*, **75**, 2689-2691

[23] V. N. Davydov, 1995, *Russ. Phys. J.*, **42**, 476-484

[24] Y. Usami, K. Imamura, T. Akai, D.-C. Che, H. Ohoyama, H. Kobayashi, and T. Matsumoto, 2016, *J. Appl. Phys.*, **120**, 084308.

[25] R. Pelster, G. Nimtz, and B. Wessling, 1994, *Phys. Rev. B*, **49**, 12718-12723.

[26] A. J. Epstein, W. P. Lee, and V. N. Prigodin, 2001, *Synth. Met.*, **117**, 9-13.

[27] D. Yu, C. Wang, B.L. Wehrenberg, and P. Guyot-Sionnest, 2004, *Phys. Rev. Lett.*, **92**, 216802.

[28] C. C. S. Pedroso, V. Junqueira, C. P. L. Rubinger, T .S. Martins, and R. Faez, 2013, *Synth. Met.*, **170**, 11-18.

[29] S.A. Travain, G.F.L. Ferreira, J.A. Giacometti, and R.F. Bianchi, 2007, *Mater. Sci. Eng. B Solid-State Mater. Adv. Technol.*, **143**, 31-37.

[30] F.N. Hooge, T.G.M. Kleinpenning, and L. K. J. Vandamme, 1981, *Reports Prog. Phys.*, **44**, 479-532.

[31] C. Liang, G. Leroy, J. Gest, L. K. J. Vandamme, and J.L. Wojkiewicz, 2009, *Synth. Met.*, **159**, 1-6.

[32] Z. Zhang, J. T. Yales, 2012, *Chem. Rev.*, **112**, 5520-5551.

[33] J. B. Roldan, F. J. Alonso. A. M. Aguilera, D. Maldonado, and M. Lanza, 2019, *J. Appl Phys.*, **125**, 147504

[34] J. Wei and V. Chandrasekhar, 2009, *Nat. Phys.*, **6**, 494-498

[35] R. Chen, F. Fan, T. Dittrich and C. Li, 2018, *Chem. Soc. Rev.*, **47**, 8238-8262

[36] N. F. Mott, 1968, *Phil. Mag.*, **19**, 835-852

[37] M. Saritas, H. D. McKell, 1988, *J. Appl. Phys*, **63**, 4561-4567.

[38] N. Honma, C. Munakata and H. Itoh, 1984, *Jpn. J. Appl. Phys.*, **23**, L354-L356

[39] V. Kolkovsky, 2019, *Phys. Status Solidi.* A, **216**, 1900310

[40] L. Collins, M. Ahmadi, J. Qin, Y. Liu, O. S Ovchinnikova, B. Hu, S. Jesse and S. V Kalinin, 2018, *Nanotechnology*, **29**, 445703

[41] K. Kajimoto, K. Araki, Y. Usami, H. Ohoyama and T. Matsumoto, In Submission